



Original Article

Radiation-hardened-by-design preamplifier with binary weighted current source for radiation detector

Minuk Seung^{a,b}, Jong-Gyun Choi^a, Woo-young Choi^b, Inyong Kwon^{c,*}^a Korea Atomic Energy Research Institute (KAERI), 989-111 Daedeok-daero, Yuseong, Daejeon, 34057, Republic of Korea^b College of Electrical and Electronic Engineering, Yonsei University, Seoul, 03722, Republic of Korea^c Department of Radiological Science, Yonsei University, Wonju, 26493, Republic of Korea

ARTICLE INFO

Keywords:

Radiation detector readout system
 Preamplifier
 Radiation-hardened-by-design
 RHBD preamplifier
 Charge-sensitive amplifier
 Binary weighted current source

ABSTRACT

This paper presents a radiation-hardened-by-design preamplifier that utilizes a self-compensation technique with a charge-sensitive amplifier (CSA) and replica for total ionizing dose (TID) effects. The CSA consists of an operational amplifier (OPAMP) with a 6-bit binary weighted current source (BWCS) and feedback network. The replica circuit is utilized to compensate for the TID effects of the CSA. Two comparators can detect the operating point of the replica OPAMP and generate appropriate signals to control the switches of the BWCS. The proposed preamplifier was fabricated using a general-purpose complementary metal-oxide-silicon field effect transistor 0.18 μm process and verified through a test up to 230 kGy (SiO₂) at a rate of 10.46 kGy (SiO₂)/h. The code of the BWCS control circuit varied with the total radiation dose. During the verification test, the initial value of the digital code was 39, and a final value of 30 was observed. Furthermore, the preamplifier output exhibited a maximum variation error of 2.39%, while the maximum rise-time error was 1.96%. A minimum signal-to-noise ratio of 49.64 dB was measured.

1. Introduction

A preamplifier is an essential component in various measurement systems because it performs the crucial function of extracting and amplifying the signal generated by the interaction between a detector and the target being measured [1]. Moreover, a preamplifier can achieve a high signal-to-noise ratio (SNR) by amplifying a weak signal and minimizing the noise [2]. A preamplifier is typically positioned at the first stage of the detector readout interface, directly influencing the overall detection efficiency and energy resolution of the system [3,4]. Preamplifier architectures vary depending on the type of signal generated by the detector, which could be a voltage type, charge type, conductive type, or resistive type [5–7]. Thus, the preamplifier should be designed to match the specific characteristics of the sensor and optimize its performance.

A charge-sensitive amplifier (CSA) is commonly used to convert the charge signal of a radiation detector into a voltage, such as in ion chambers, scintillators, and fission detectors, as shown in Fig. 1 [8,9]. The conventional CSA consists of an operational amplifier (OPAMP), feedback resistor (R_F), and feedback capacitor (C_F). The CSA output is directly proportional to the amount of input charge (Q_{in}), as determined

by Eq. (1).

$$V_{out} = -A_V \frac{Q_{in}}{C_{det} + (A_V + 1)C_F} \quad (1)$$

Here, A_V is the open loop gain of the OPAMP, and C_{det} is the detector capacitance. If the detector capacitance is lower than $(A + 1)C_F$, the output voltage can be found using (2) [8–10].

$$V_{out} = -\frac{Q_{in}}{C_F} \quad (2)$$

The performance of a CSA, which uses silicon semiconductor devices, degrades as a result of radiation effects, which can occur in various radiation environments, including nuclear power plants (NPPs), military settings, space, and radiation therapy applications [11–15]. Two types of effects can occur in irradiated semiconductor devices: single event effects (SEEs) and total ionization dose (TID) effects. SEEs are mainly generated by high-energy particles such as neutrons, protons, and alpha particles [12]. Thus, SEEs are primarily a concern in the space industry. SEEs cause two types of errors. Soft errors can flip over digital bits in data storage such as D flip flop (DFF) and static random-access memory (SRAM) components in high-energy radiation fields like the space

* Corresponding author.

E-mail address: ikwon@yonsei.ac.kr (I. Kwon).

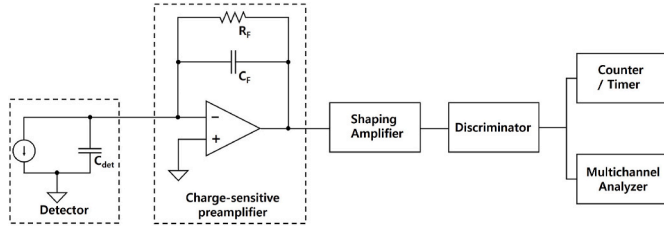


Fig. 1. System diagram of a radiation detector. Charge-sensitive amplifier extracts signal from detector and amplifies the signal. The amplified signal is then transmitted to a shaping amplifier and discriminator for signal processing.

environment [13]. Hard errors, including single event latch-up (SET), single event burnout (SEB), and single event gate rupture (SEGR), permanently damage a MOSFET and then cause a system operating failure [14]. Because TID effects are a cumulative phenomenon, electrical circuits used in environments with continuous radiation exposure are susceptible to the effects. Electron–hole pairs (EHPs) are generated when radiation interacts with the oxide region of a semiconductor, depending on the deposited energy in the oxide region, such as gate oxide and shallow trench isolation (STI) [16]. Most of the generated EHPs recombine promptly in the dielectric region, but some electrons escape from the dielectric region, whereas holes are trapped within the SiO₂ and SiO₂–Si interface as a result of the difference in mobility between electrons and holes [17]. If a hole is trapped at the gate oxide region, it can cause a threshold voltage shift. On the other hand, if a hole is trapped at the STI region, it creates an additional current path, causing an increase in the leakage current [18–20]. The radiation-induced leakage current occurs degradation of the transconductance, accumulation of the charge on the circuit node, and increase of the static power [21]. Radiation detectors employed in NPPs might be subjected to continuous radiation exposure, especially in severe accident scenarios, with a rate of 230 Gy/h [22]. As a result, the instrumentation system becomes vulnerable to TID effects, potentially leading to the generation of inaccurate information.

Previous research primarily focused on enhancing the tolerance for radiation effects through specific semiconductor device structures known as silicon-on-insulator (SOI), silicon-on-sapphire (SOS), and the enclosed layout transistor (ELT). These methods are called radiation-hardening-by-process [[16–19,23]]. SEEs are effectively minimized by the SOI and SOS processes, including the SEU and SEL [16]. The ELT structure does not have an edge that can cause a parasitic channel when radiation penetrates the CMOS [23]. It has already been verified that a radiation-hardened structure has low sensitivity to TID effects [24]. However, the ELT structure is subject to several drawbacks such as low area efficiency, which is three times larger than conventional devices [23], as well as challenges in designing the layout and conducting electrical verification tests because of the unavailability of a process design kit (PDK) from fabrication companies [4].

Recently, research on mitigating radiation effects through the radiation-hardened-by-design (RHBD) approach has been actively conducted. The RHBD approach is a technique that enhances stability and reliability in radiation environments by implementing structural designs at the circuit level, rather than the transistor device level, to alleviate TID effects. Differential charge cancellation (DCC) [25], sensitive node active charge cancellation (SNACC) [26], and three error detection techniques of over- and under-flow, extra bit, and parity bit [27] have been reported for mitigating SEEs. Additionally, channel width optimization [4], dynamic-threshold MOS transistors (DTMOSTs) [16], chopper stabilization [28], and first-order cancellation techniques [29] have been reported for minimizing TID effects. The limitations of using the ELT structure can be overcome by employing the RHBD technique. Therefore, this article presents an RHBD technique that utilizes a replica circuit to detect TID effects and compensate for degradations caused by radiation without an ELT structure.

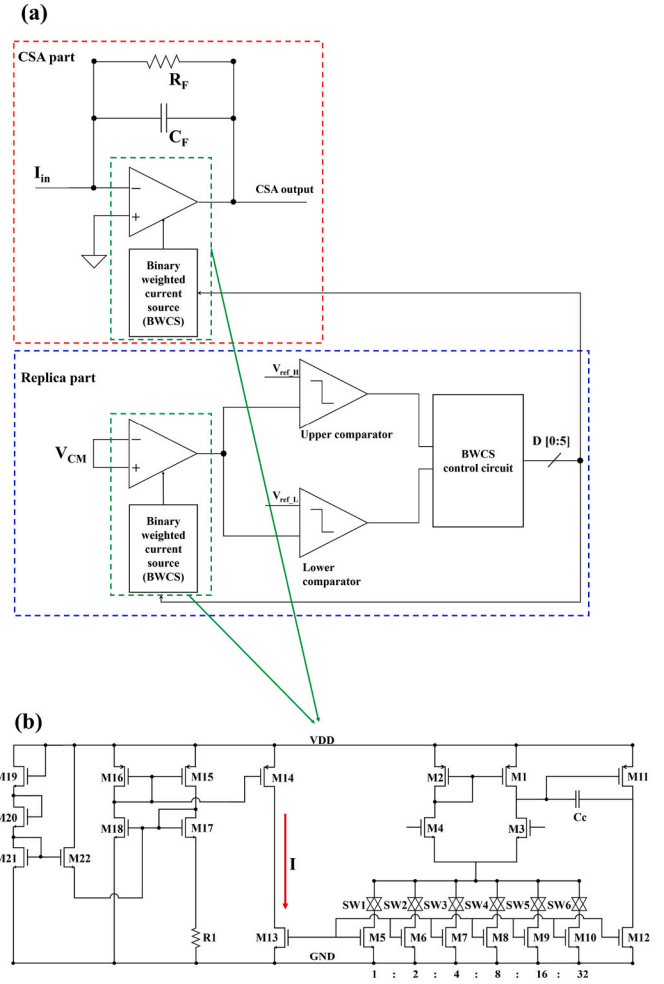


Fig. 2. (a) Block diagram of proposed preamplifier. The proposed preamplifier consists of two parts: the CSA and replica. (b) Configuration of two-stage OPAMP used for proposed preamplifier. The OPAMP has a 6-bit binary weighted current source (BWCS) to compensate for TID effects.

2. Circuit implementation

2.1. Strategy for radiation hardening

The strategy for radiation hardening involves compensating for changes in the current level of the preamplifier to minimize TID effects by using a 6-bit binary weighted current source (BWCS). The preamplifier was designed using a two-stage OPAMP, which is well known for its high speed, low noise, low power, and proper gain. The open loop gain and gain-bandwidth product (GBWP) of the two-stage OPAMP can be found using (3) and (4), respectively:

$$A_V = -g_{m3}g_{m11}(r_{o1} / r_{o3})(r_{o11} / r_{o12}), \quad (3)$$

$$GBWP \approx \frac{g_{m3}}{C_c}, \quad (4)$$

where g_m is the transconductance, r_o is the output resistance, and C_c is the Miller capacitance. The transconductance and output resistance are properties of the MOSFET, which are determined using (5) and (6), respectively:

$$g_m = \frac{2I_D}{V_{OV}}, \quad (5)$$

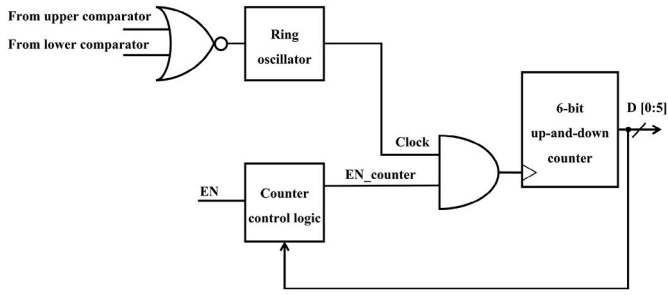


Fig. 3. Configuration of the BWCS control circuit. The circuit consists of a ring oscillator, counter control logic, and a 6-bit up-and-down counter.

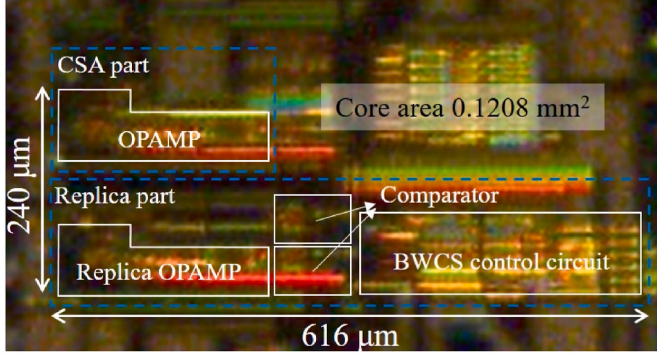


Fig. 4. Photograph of the proposed preamplifier circuit in 0.18 μm standard CMOS technology.

$$r_o = \frac{1}{\lambda I_D}, \quad (6)$$

where I_D is the drain current; V_{OV} represents the overdrive voltage, which is defined as the difference between the gate-source voltage and threshold voltage of the MOSFET; and λ is the channel length modulation coefficient. As previously mentioned, the circuit properties vary as a result of the radiation, including a threshold voltage shift, leakage current increase, and noise increase. In modern CMOS processes, particularly sub-micrometer fabrication, the impact on circuits of a threshold voltage shift induced by radiation is gradually decreasing. This can be attributed to the reduction in the oxide region thickness (t_{ox}) [16] because the threshold shift is proportional to t_{ox}^2 . Furthermore, a thin oxide layer enhances the quantum tunneling effect [20]. Consequently, the recombination process for EHPs can occur at a higher frequency. In contrast, as circuits are scaled down and the current level of the circuit system decreases, the influence of leakage current becomes more dominant [20]. Thereby, in (4) and (5), the variation of I_D can contribute more significantly to the fluctuations of g_m and r_o . Therefore, maintaining the current level of the system is necessary to mitigate fluctuations in g_m regardless of the presence of radiation effects.

2.2. Circuit description

The proposed preamplifier, which is depicted in Fig. 2 (a), is composed of two main parts: the CSA and replica. The CSA of the proposed preamplifier includes an OPAMP with a 6-bit BWCS, and a feedback network that operates as the CSA for radiation detectors. The replica of the preamplifier was designed to compensate for TID effects and consists of an OPAMP with the same schematic used for the CSA, two conventional continuous comparators, and a BWCS control circuit. The two-stage OPAMP configuration is used in the proposed preamplifier, which consists of a self-bias circuit, transmission gates, and a 6-bit BWCS, as illustrated in Fig. 2 (b). The RHBD technique could

Table 1

Electrical parameters of the two-stage OPAMP with 6-bit BWCS.

Parameters (unit)	Value
Supply voltage (V)	1.8
Miller capacitance (pF)	1
Open loop gain (dB)	66
3 dB BW (kHz)	112.5
GBWP (MHz)	217.15
Phase margin ($^\circ$)	55

significantly improve the system's performance and enhance its reliability, particularly when utilized in radiation environments. The BWCS control circuit is composed of a ring oscillator, a 6-bit up-and-down counter, and counter control logic, as depicted in Fig. 3. The BWCS can supply current to the OPAMP in the proposed preamplifier in the range of 1 I to 64 I, depending on the output signal of the BWCS control circuit. By utilizing the self-compensation technique for the current supplied by the BWCS, the proposed preamplifier can mitigate changes in current induced by radiation effects.

The RHBD preamplifier was implemented in a general-purpose complementary metal-oxide-silicon field effect transistor (MOSFET) 0.18 μm technology process. A photograph of the fabricated chip is shown in Fig. 4. The active area of the proposed circuit occupies 0.1208 mm^2 . Table 1 lists the electrical specifications of the OPAMP for the proposed preamplifier.

2.3. Operating principle of self-compensation technique

The replica OPAMP in the replica part acts as a sensor that is capable of detecting current variations caused by TID effects. Under normal conditions, when the OPAMP is supplied with a common-mode voltage at its inputs, the output should also be maintained at the common-mode level. However, when the circuit is exposed to radiation, the OPAMP shows fluctuations in its current, resulting in a shift in its operating point. These changes in the current level can be detected by employing two comparators with appropriate reference voltages. The two reference voltages are set near the common mode voltage of the OPAMP. To account for the possibility of variations due to noise, they are set at ± 200 mV from the common mode voltage. As a result, when the common mode voltage shifts, greater or smaller than the reference voltages, each comparator can generate a HIGH signal. Depending on the signal generated by either the upper or lower comparator, the counter can operate as either an up-counter or a down-counter. For instance, if the radiation effect causes an increase in the operating point of the replica, the upper comparator generates the HIGH signal and the 6-bit up-and-down counter operates as a down counter to reduce the current of the system. On the other hand, if the output decreases, the lower comparator generates the HIGH signal and the counter acts as an up counter to increase the current of the preamplifier. The digital logic generates signals that control the switches in the BWCS in both OPAMPs. Therefore, the proposed preamplifier can compensate for any degradation induced by TID effects by maintaining the current level of the OPAMP.

The ring oscillator in the BWCS control circuit generates a sufficiently wide pulse with a duration of 1.9 μs , which serves as the clock signal for the counter. If the clock signal is faster than the propagation delay of the BWCS system, the next clock cycle may enter the counter before the BWCS code is changed. In that case, multiple clocks are counted by the counter within the same phase.

The operation of the counter should be halted upon meeting specific conditions such as reaching the state of saturation at 000001 or 111111. Because the counter operates cyclically, failure to terminate its operation at saturation points would result in an infinite cycle, spanning from 000000 to 111111. For instance, when the output of the counter is 111111, if the lower comparator generates a signal, then the output of the counter will transition to 000000, indicating a significant decrease in

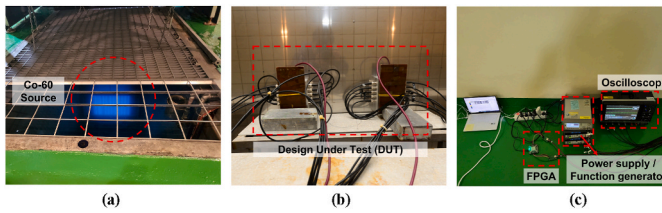


Fig. 5. (a) Cobalt-60 gamma ray source for irradiation test. (b) DUT board and (c) electrical equipment for experiment.

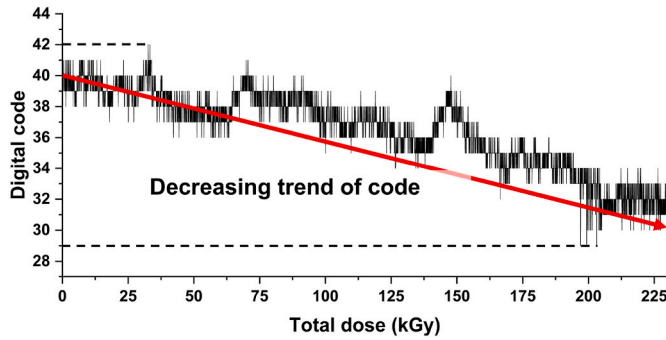


Fig. 6. Trend curve for output of the BWCS control circuit in relation to the total dose. As the total dose increases, the graph exhibits a downward trend. An initial value of 39, a maximum value of 42, and a minimum value of 29 were recorded.

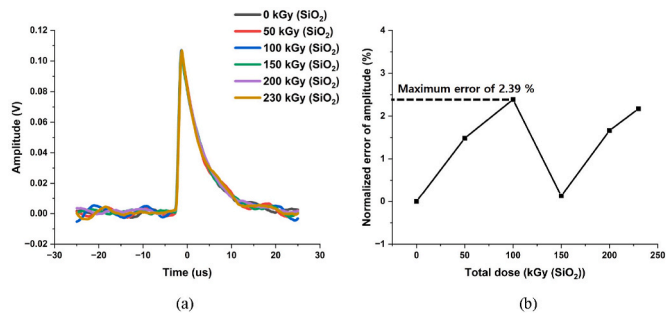


Fig. 7. During irradiation test with gamma rays up to 230 kGy (SiO₂): (a) recorded output of CSA and (b) error rate of normalized amplitude of the preamplifier obtained as a maximum error rate of 2.39%.

the current level of the preamplifier from 64 I to 1 I. This situation can potentially indicate a malfunction in the preamplifier system. Therefore, the arbiter circuit is designed to control the operation of the counter by utilizing logic gates when it is saturated.

3. Verification

A verification test of the radiation hardening was conducted at the Korea Atomic Energy Research Institute (KAERI) using a cobalt-60 gamma-ray source up to 230 kGy (SiO₂) at a rate of 10.46 kGy (SiO₂)/h. Fig. 6 shows the test environment. Fig. 5 (a) shows the radiation source, which was submerged in water and then raised to the surface when the experiment began. The design under test (DUT) board was placed in front of the radiation source as displayed in Fig. 5 (b). All the electrical equipment was positioned behind a 30 cm concrete wall to avoid radiation effects, as illustrated in Fig. 5 (c). The equipment and DUT were connected using 15 m cables. Two types of data were captured for analysis: analog data from the output of the CSA, which was recorded using an oscilloscope, and digital data from the output of the BWCS control circuit, which was logged using an FPGA. The data were stored

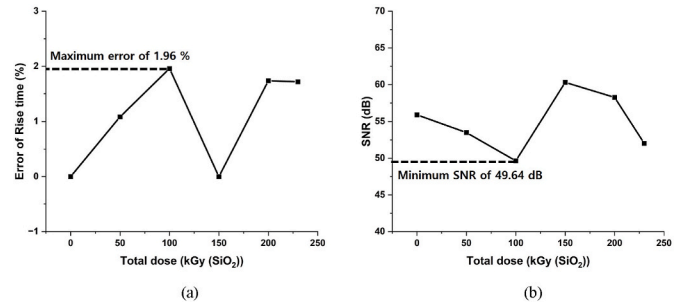


Fig. 8. During irradiation test with gamma rays up to 230 kGy (SiO₂): (a) maximum rise time of 0.588 μs and (b) SNR in range of 49.64 dB–60.31 dB.

at regular intervals of 20 s.

Fig. 6 depicts the changes in the output of the BWCS control circuit during the irradiation test. According to the experimental results, the digital code had a maximum value of 42 and a minimum value of 29 during the irradiation test, whereas it had an initial value of 39 before the test. The results indicated that the system current level tended to decrease as a result of radiation effects. This phenomenon might have been related to the leakage current increase. When the leakage current increased, the system current level also increased. Thus, the BWCS was able to decrease the system current. The small and regional variation in the code could have occurred as a result of a quantization error caused by the current changing in increments of 1 I. In other words, because the system required a value between two specific codes, a fluctuation error occurred.

Fig. 7 (a) displays the output of the preamplifier at 50 kGy (SiO₂) intervals during the irradiation test. Variations in the amplitude of the output could occur as a result of changes in the open-loop gain, as shown in (1). As previously discussed, the open-loop gain was determined by the transconductance and output resistance of the OPAMP. Radiation effects could cause changes in the current level of the system, resulting in fluctuations in the system’s gain. Fig. 7 (b) depicts the error rate of the normalized maximum amplitude of the proposed preamplifier. A maximum error of 2.39% was observed at 100 kGy (SiO₂), with the digital code reaching 38.

Fig. 8 (a) shows the rise time variation during the gamma-ray exposure test. It was calculated at 20% and 80% of the peak voltages, avoiding the impact of the noise. The rise time was measured as 0.577 μs before the irradiation test. A maximum rise time of 0.588 μs was observed, along with an error of 1.96% at a total dose of 100 kGy (SiO₂). The rise time variation was also related to the system current level because the slew rate was obtained using (7) [3].

$$Slew\ rate = \frac{C_c}{I_D} \tag{7}$$

The SNR exhibited a range of 49.64 dB–60.31 dB, depending on the total radiation dose, as illustrated in Fig. 8 (b). The SNR is a crucial parameter for a preamplifier because it quantifies the noise level relative to the readout system signal. It provides a measure of the ability to distinguish the desired signal from the unwanted noise originating from the detectors. The gate-referred noise voltage spectrum is represented by (8):

$$S_c^2(f) = 4kT \frac{\alpha}{g_m} + \frac{K_f}{C_{ox}WL} \frac{1}{f} \tag{8}$$

The first term is the thermal noise term. k is the Boltzmann constant, T is the absolute temperature, and α is the channel’s thermal noise coefficient. Thus, the degradation of the transconductance results in an increase in noise within the circuit [30]. The second term is the flicker noise term (1/f) [19]. K_f is intrinsic process parameter, C_{ox} is the gate capacitance. As previous studies, 1/f noise is also affected by radiation, resulting variation of K_f [20]. As the test result, the maximum error rate

Table 2
Comparison results of RHBD OPAMPs.

Technology	This work	[3]		180 nm Si CMOS		180 nm Si BiCMOS	
	180 nm Si CMOS	130 nm SiGe CMOS		Basic	Double width	Tail current (50 μ A)	Tail current (67 μ A)
Amplitude variation (%)	2.39	3.6	2.23	2.85	2.32	34.3	16.17
SNR variation (dB)	−5.74–4.92	−0.314	−0.202	2.396	0.07	11.6	3.12
Gain (dB)	66	41.9	42.3	39.37	38.83	62.43	62.43
GBWP (MHz)	217.15	316.2	377.3	202.25	289.5	115.24	115.24
Phase margin (°)	55	56	57	58	57	44	44
SNR (dB)	55.38	29.6	29.2	28.25	28.75	37	31
Maximum dose	230 kGy (SiO ₂)	20 kGy (SiO ₂)					

of the SNR, in terms of its absolute value, was measured at 11.2% when subjected to a total radiation dose of 100 kGy (SiO₂).

Table 2 shows comparison result in terms of amplitude variation, SNR variation, maximum dose, and the specifications of the OPAMP used for CSA. In Ref. [3], they conducted an analysis of the radiation effects on the CSA configured with a conventional two-stage OPAMP. They considered three types of processes: SiGe CMOS, Si CMOS, and Si BiCMOS technologies, while also varying MOSFET channel size and system current levels. The term “basic” refers to the conventional two-stage OPAMP structure for the CSA, while “double width” indicates an OPAMP configuration with transistors having twice the width of the basic circuit. The “tail current” signifies the current level flowing through the OPAMP. As comparison results, the proposed CSA is observed that there is less variation in the amplitude at higher dose. Although the proposed circuit experienced greater SNR degradation due to radiation, its inherent circuit SNR is significantly higher, resulting in even the lowest SNR of proposed CSA being greater compared to the highest SNR of [3].

4. Conclusion

A radiation-hardened preamplifier was introduced for the radiation detectors used in NPPs. The RHBD preamplifier can mitigate radiation-induced degradations, particularly TID effects, by compensating the tail current of the OPAMP used for the preamplifier using a 6-bit BWCS, through which a wide range of current (1 I to 64 I) can flow. The replica OPAMP of the proposed preamplifier detects the changes in the operating point caused by the total radiation dose and generates a signal to control the BWCS, aiming to minimize TID effects. The circuit was fabricated using the 0.18 μ m CMOS process, and occupied 0.1208 mm². An irradiation test was performed using a gamma-ray source up to 230 kGy (SiO₂) at a rate of 10.46 kGy (SiO₂)/h. Degradations were observed, and the gain and rise time were compensated. The gain had a maximum error of 2.39% at a total radiation dose of 100 kGy (SiO₂). The rise time had a maximum value of 0.588 μ s with an error of 1.96% at the total radiation dose of 100 kGy (SiO₂). The measured SNR had a minimum value of 49.64 dB. Therefore, the RHBD preamplifier could be used in various sensor applications, particularly radiation environments, because the proposed circuit could maintain its performance regardless of increased radiation exposure.

Declaration of competing interest

The authors declare that they have no known competing financial interests or personal relationships that could have appeared to influence the work reported in this paper.

Acknowledgments

This work was supported in part by the Basic Science Research Program through the National Research Foundation of Korea (NRF) funded by the Ministry of Science and ICT (RS-2022-00144419 and

2022M3F3A2A01072851).

References

- [1] M. Jeong, G. Kim, Development of charge sensitive amplifiers based on various circuit board substrates and evaluation of radiation hardness characteristics, *Nucl. Eng. Technol.* 52 (7) (2020) 1503–1510.
- [2] M. Massarotto, A. Carlosena, A.J. Lopez-Martin, Two-stage differential charge and transresistance amplifiers, *IEEE Trans. Instrum. Meas.* 57 (2) (2008) 309–320.
- [3] C. Lee, G. Cho, T. Unruh, S. Hur, I. Kwon, Integrated circuit design for radiation-hardened charge-sensitive amplifier survived up to 2 Mrad, *Sensors* 20 (10) (2020).
- [4] H. Jeon, I. Kwon, M. Je, Radiation-hardened sensor interface circuit for monitoring severe accidents in nuclear power plants, *IEEE Trans. Nucl. Sci.* 67 (7) (2020) 1738–1745.
- [5] G. Langfelder, A. Caspani, A. Tocchio, Design criteria of low-power oscillators for consumer-grade MEMS resonant sensors, *IEEE Trans. Ind. Electron.* 61 (1) (2014) 567–574.
- [6] B. George, Z. Tan, S. Nihtianov, Advances in capacitive, eddy current, and magnetic displacement sensors and corresponding interfaces, *IEEE Trans. Ind. Electron.* 64 (12) (2017) 9595–9607.
- [7] J. Kim, Y.B. Kim, D.-Y. Seok, S.Y. Lee, J.Y. Sim, H.R. Choi, Performance enhancement of capacitive-type torque sensor by using resonant circuit, *IEEE Trans. Ind. Electron.* 69 (1) (2022) 560–569.
- [8] I. Kwon, T. Kang, B.T. Wells, L.J. D’Aries, M.D. Hammig, Compensation of the detector capacitance presented to charge-sensitive preamplifiers using the Miller effect, *Nucl. Instrum. Methods Phys. Res. Sect. A Accel. Spectrom. Detect. Assoc. Equip.* 784 (2015) 220–225.
- [9] I. Kwon, T. Kang, M.D. Hammig, Experimental validation of charge-sensitive amplifier configuration that compensates for detector capacitance, *IEEE Trans. Nucl. Sci.* 63 (2) (2016) 1202–1208.
- [10] G.F. Knoll, *Radiation Detection and Measurement*, WILEY, New Jersey, 2010.
- [11] T.S. Nidhin, A. Bhattacharyya, R.P. Behera, T. Jayanthi, K. Velusamy, Understanding radiation effects in SRAM-based field programmable gate arrays for implementing instrumentation and control systems of nuclear power plants, *Nucl. Eng. Technol.* 49 (8) (2017) 1589–1599.
- [12] C. Sharma, P. Rajesh, R.P. Behera, S. Amirthapandian, Impact of gamma radiation on 8051 microcontroller performance, *Nucl. Eng. Technol.* 54 (12) (2022) 4422–4430.
- [13] H.J. Barnaby, Total-ionizing-dose effects in modern CMOS technologies, *IEEE Trans. Nucl. Sci.* 53 (6) (2006) 3103–3121.
- [14] J.D. Cressler, *Extreme Environment Electronics*, CRC press, Florida, 2013.
- [15] W. Yang, Y. Li, G. Guo, C. He, L. Wu, System-on-chip single event effect hardening design and validation using proton irradiation, *Nucl. Eng. Technol.* 55 (3) (2023) 1015–1020.
- [16] V. Gromov, A.J. Annema, R. Kluit, J.L. Visschers, P. Timmer, A radiation hard bandgap reference circuit in a standard 0.13 μ m CMOS technology, *IEEE Trans. Nucl. Sci.* 54 (6) (2007) 2727–2733.
- [17] B.M. McCue, et al., A Wide Temperature, Radiation Tolerant, CMOS-compatible precision voltage reference<newline/>for extreme radiation environment <newline/>Instrumentation Systems, *IEEE Trans. Nucl. Sci.* 60 (3) (2013) 2272–2279.
- [18] V. Re, M. Manghisoni, L. Ratti, V. Speziali, G. Traversi, Total ionizing dose effects on the noise performances of a 0.13 μ m CMOS technology, *IEEE Trans. Nucl. Sci.* 53 (3) (2006) 1599–1606.
- [19] M. Manghisoni, L. Ratti, V. Re, V. Speziali, G. Traversi, A. Candelori, Comparison of ionizing radiation effects in 0.18 and 0.25 μ m CMOS technologies for analog applications, *IEEE Trans. Nucl. Sci.* 50 (6) (2003) 1827–1833.
- [20] D.M. Colombo, A. Rosseto, G.I. Wirth, S. Bampi, O.L. Gonzalez, Total dose effects on voltage references in 130-nm CMOS technology, *IEEE Trans. Device Mater. Reliab.* 18 (1) (2018) 27–36.
- [21] J.D. Cressler, H.A. Mantooth, *Environments and prediction tools*, in: *Extreme Environment Electronics*, first ed., CRC Press, Boca Raton, Florida, USA, 2013.
- [22] IAEA TECDOC Series, Assessment of equipment capability to perform reliability under severe accident conditions, IAEA-TECDOC-1818. Available: https://www-pub.iaea.org/MTCD/Publications/PDF/TE-1818_web.pdf.
- [23] W.J. Snoeys, T.A.P. Gutierrez, G. Anelli, A new NMOS layout structure for radiation tolerance, *IEEE Trans. Nucl. Sci.* 49 (4) (2002) 1829–1833.

- [24] T. Vergine, M. De Matteis, S. Michelis, G. Traversi, F. De Canio, A. Baschiroto, A 65 nm rad-hard bandgap voltage reference for LHC environment, *IEEE Trans. Nucl. Sci.* 63 (3) (2016) 1762–1767.
- [25] R.W. Blaine, et al., Single-event-hardened cmos operational amplifier design, *IEEE Trans. Nucl. Sci.* 59 (4) (2012) 803–810.
- [26] Atkinson, et al., RHBD technique for single-event charge cancellation in folded-cascode amplifiers, *IEEE Trans. Nucl. Sci.* 60 (4) (2013) 2756–2761.
- [27] H. Xu, et al., A 78.5-dB SNDR radiation- and metastability-tolerant two-step split SAR ADC operating up to 75 MS/s with 24.9-mW power consumption in 65-nm CMOS, *IEEE J. Solid State Circ.* 54 (2) (2019) 441–451.
- [28] K.J. Shetler, et al., Radiation hardening of voltage references using chopper stabilization, *IEEE Trans. Nucl. Sci.* 62 (6) (2015) 3064–3071.
- [29] M. Seung, W. Choi, S. Hur, I. Kwon, Cold junction compensation technique of thermocouple thermometer using radiation-hardened-by-design voltage reference for harsh radiation environment, *IEEE Trans. Instrum. Meas.* 71 (2022) 1–7.
- [30] M. Manghisoni, L. Ratti, V. Speziali, Submicron CMOS technologies for low-noise analog front-end circuits, *IEEE Trans. Nucl. Sci.* 49 (4) (2022) 1783–1790.